**Special Issue Article**
**Smart nanophotonics for renewable energy and sustainability**

**Open Access**

Yixuan Tan, Baoan Liu, Sheng Shen, and Zongfu Yu

# Enhancing radiative energy transfer through thermal extraction

DOI 10.1515/nanoph-2016-0008
Received September 30, 2015; accepted January 12, 2016

**Abstract:** Thermal radiation plays an increasingly important role in many emerging energy technologies, such as thermophotovoltaics, passive radiative cooling and wearable cooling clothes [1]. One of the fundamental constraints in thermal radiation is the Stefan-Boltzmann law, which limits the maximum power of far-field radiation to $P_0 = \sigma T^4 S$, where $\sigma$ is the Boltzmann constant, $S$ and $T$ are the area and the temperature of the emitter, respectively (Fig. 1a). In order to overcome this limit, it has been shown that near-field radiations could have an energy density that is orders of magnitude greater than the Stefan-Boltzmann law [2–7]. Unfortunately, such near-field radiation transfer is spatially confined and cannot carry radiative heat to the far field. Recently, a new concept of thermal extraction was proposed [8] to enhance far-field thermal emission, which, conceptually, operates on a principle similar to oil immersion lenses and light extraction in light-emitting diodes using solid immersion lens to increase light output [62].Thermal extraction allows a blackbody to radiate more energy to the far field than the apparent limit of the Stefan-Boltzmann law without breaking the second law of thermodynamics.

Thermal extraction works by using a specially designed thermal extractor to convert and guide the near-field energy to the far field, as shown in Fig. 1b. The same blackbody as shown in Fig. 1a is placed closely below the thermal extractor with a spacing smaller than the thermal wavelength. The near-field coupling transfers radiative energy with a density greater than $\sigma T^4$. The thermal extractor, made from transparent and high-index or structured materials, does not emit or absorb any radiation. It transforms the near-field energy and sends it toward the far field. As a result, the total amount of far-field radiative heat dissipated by the same blackbody is greatly enhanced above $S\sigma T^4$, where $S$ is the area of the emitter. This paper will review the progress in thermal extraction. It is organized as follows. In Section 1, we will discuss the theory of thermal extraction [8]. In Section 2, we review an experimental implementation based on natural materials as the thermal extractor [8]. Lastly, in Section 3, we review the experiment that uses structured metamaterials as thermal extractors to enhance optical density of states and far-field emission [9].

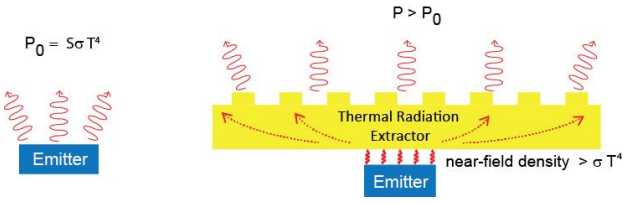


**Figure 1:** Schematic of radiative cooling. (Left) Emitter without thermal extractor. (Right) Radiation power of emitter with thermal extractor is larger than that on the left.

## 1 Thermal Extraction Theory

We start by considering the classical construction of an ideal blackbody emitter: a small opening in a cavity as shown in Fig. 2. The cavity is filled with transparent dielectric medium that has a refractive index $n_i$ as shown in Fig. 2a. Outside the cavity is vacuum. Inside the cavity, the sidewalls are made of diffusive reflector that also absorbs light. Any light that enters through the open area will bounce back and forth between the sidewalls and eventually get fully absorbed by the cavity. Here we assume perfect antireflection at the opening of the cavity. The cavity's temperature is $T$ and its opening area has an area of $S$. The opening area is completely dark with a unity emissivity.

We will investigate the thermal emission when the cavity is filled by materials of different refractive indices $n_i$. As we vary $n_i$, the thermal radiation intensity inside the cavity

**Yixuan Tan, Zongfu Yu:** Department of Electrical and Computer Engineering, University of Wisconsin, Wisconsin, Madison, 53706, USA
**Baoan Liu, Sheng Shen:** Department of Mechanical Engineering, Carnegie Mellon University, Pittsburgh, PA, 15213, USA

BY-NC-ND © 2016 Yixuan Tan et al., published by De Gruyter Open.
This work is licensed under the Creative Commons Attribution-NonCommercial-NoDerivs 3.0 License.

Brought to you by | University of Wisconsin Madison Libraries
Authenticated
Download Date | 6/3/16 6:36 PM

scales as $n_i^2$. However, the cavity always has the same far-field thermal emission with an emitted power of $\sigma T^4 S$ [37]. This is because the total internal reflection at the opening of the cavity prevents a significant portion of the internal thermal radiation from leaving the cavity. The resulting thermal emission to the far-field vacuum always has the same profile independent of refractive index $n_i$.

To extract more radiation power from this type of a structure, Yu, et al. [8] proposed to place a hemispherical dome to cover the cavity, as shown in Fig. 2 b. Here the dome has an index $n_e$. It enlarges the critical angle for totally internal reflection at the cavity opening and thus enables more thermal radiation modes inside the cavity to escape. Importantly, the dome itself is assumed to be transparent, so that it neither emits nor absorbs any thermal radiation.

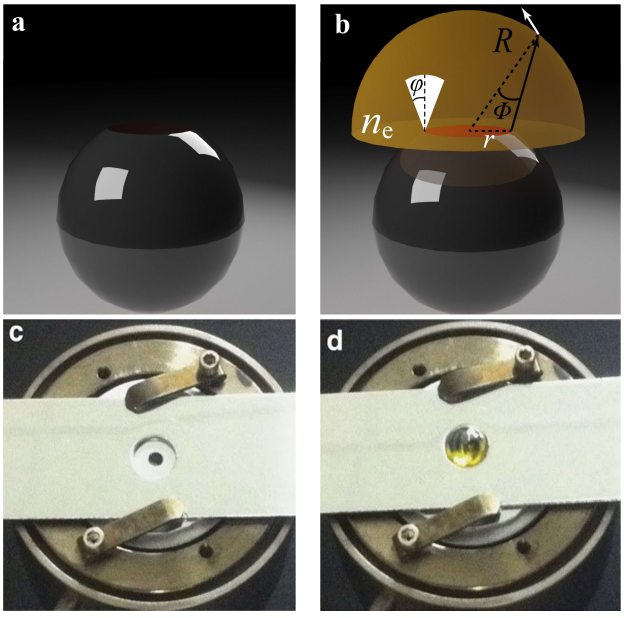


**Figure 2:** Schematic and actual demonstration of thermal extraction. (a) Emitter formed by an open area (dark red surface) of an absorptive cavity. The cavity can be filled with a transparent dielectric of refractive index $n_i$. (b) Thermal extraction using a hemispherical dome placed at the opening of the cavity. The dome is transparent and does not emit or absorb any thermal radiations, and has a refractive index $n_e$. Emission cone (white) of the thermal radiation inside the dome is shown. (c, d) [8] Experiment set-up.

A ray tracing method can be used to calculate the thermal emission from the geometry shown in Fig. 2b. It is assumed that the opening of the cavity has a circular shape of radius $r$ and the dome has a radius $R$ such that $R > n_e r$, which ensures that any light reaching the surface of the dome can escape to the far field vacuum. Under such conditions, a light ray originating from the open area S, has an incident angle less than the total internal reflection angle $\varphi \le \sin^{-1}(\frac{1}{n_e})$ (Fig. 2b, solid arrows) at the curved interface between the dome and the outside vacuum. It can be shown that the total emission power is

$$P = \begin{cases} n_e^2 \sigma T^4 \pi r^2 \ (if\ n_i > n_e) \\ n_i^2 \sigma T^4 \pi r^2 \ (if\ n_i \le n_e) \end{cases} \quad (1)$$

Fig. 3 shows the thermal radiation as a function of the refractive index of the dome $n_e$. The total radiation power from an empty cavity ( $n_i = 1$ dashed line in Fig. 3) does not change as a function of $n_e$, while the power from the filled cavity (solid line in Fig. 3) increases as $n_e$ increases until $n_e = n_i$. With the assistance of the thermal extraction, the filled cavity can emit up to $n_i^2 S\sigma T^4$ to far-field vacuum, $n_i^2$ times of the radiated power without the thermal extractor. The internal density of the state of the thermal body must be higher than that of the extraction device in order to achieve the maximum effect of the enhanced thermal emission.

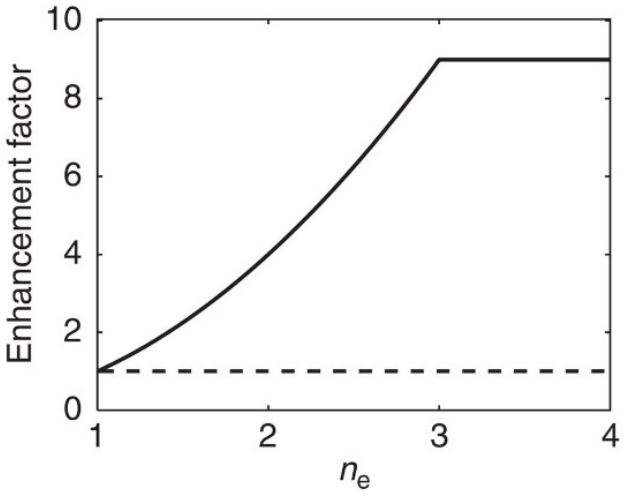


**Figure 3:** Enhancement of far-field radiation power as a function of the refractive index of the dome $\mathbf{n_e}$. Enhancement is compared with $\sigma T^4 S$. The structure for enhancement is shown in Fig. 2b. Solid line: Filled cavity with $n_i = 3$. Dashed line: Empty cavity with $n_i = 1$ [8].

The distribution of thermal radiation on the surface of the dome can be calculated with a schematic shown in Fig. 4a. For a small area $\Delta A$ on the surface of the dome, the thermal radiation power it receives from the cavity is

$$v_{\Delta A} = \Delta A \sigma T^4 \int_{\varphi<\varphi_i} \int_{x^2+y^2\le r^2} \cos(\varphi)\cos(\phi)\, n_e^2 \frac{dxdy}{\pi d^2} \quad (2)$$

The definitions of the geometric parameters in Eq. (2) are provided in Fig. 4a and $\varphi_i$ is the maximum apex angle of the emission cone. All radiation that the area $\Delta A$ receives

Brought to you by | University of Wisconsin Madison Libraries
Authenticated
Download Date | 6/3/16 6:36 PM

can escape the dome. As a dimensionless quantity, a normalized power distribution

$$f(\theta) \equiv \frac{v_{\Delta A}}{\Delta A \sigma T^4} \quad (3)$$

is defined to describe the power distribution on the surface of the dome. Owing to rotational symmetry, $f$ only depends on the polar angle $\theta$.

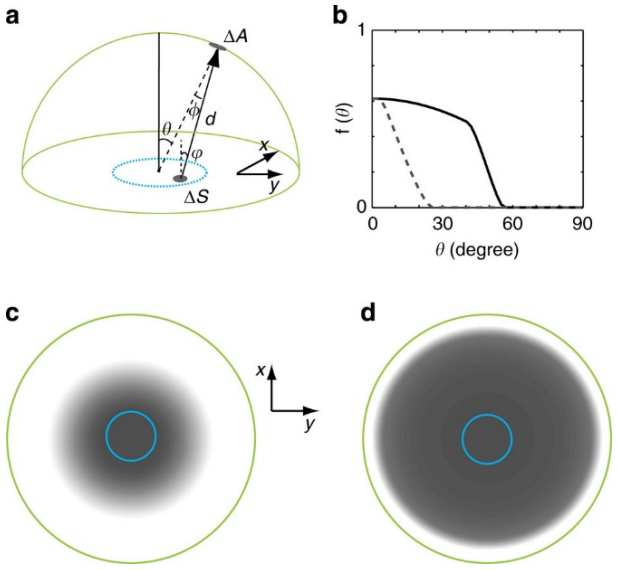


**Figure 4:** Distribution of thermal radiation on the surface of the extraction dome. (a) Schematic of the calculation. Solid arrow indicates radiation that is emitted from a small area $\Delta$S on the cavity opening and is received by a small area $\Delta$A on the surface of the dome. (b) Distribution of the radiation power on the surface of the dome as a function of the polar angle y. Dashed and solid lines are for the cases with empty and filled cavities, respectively. (c, d) The distribution of the radiation power, plotted on the hemisphere of the dome, for the case of empty (c) and filled (d) cavity. The blue circle indicates the emitter area, that is, the opening area of the cavity. The green circle is the boundary of the dome. The darker region indicates higher emission and the white region has zero emission [8].

As one specific numerical example, a case where $n_e$ = 4 is calculated. The dome radius R = 5r is chosen to satisfy the condition R > $n_e$r. $f(\theta)$ is numerically evaluated using Eq. (3) and is shown in Fig. 4b for both empty cavity ($n_i$= 1) (Fig. 4c), and filled cavity ($n_i$= 3) (Fig. 4d). For both cases, $f(\theta)$ never exceeds unity. This is expected from the Stefan-Boltzmann law, as the dome is in direct contact with vacuum outside, the emission from every surface element of the dome cannot exceed that of a surface element on a blackbody with the same area.

We see that $f(\theta)$ maximizes at normal direction $\theta$ = 0, as this area is directly above the opening the cavity. $f(\theta)$ decreases as $\theta$ increases and eventually vanishes for large $\theta$, as at large $\theta$ the corresponding area lies outside the emission cone of cavity. However, the emission profile of the filled cavity expands to a much wider angular range than that of the empty cavity (Fig. 4c,d). When thermal extraction occurs, as an example for the case here of the filled cavity, the entire dome appears bright. Therefore, the use of the transparent dome allows one to enlarge the actual emission area beyond the physical area of the emitter itself and, therefore, enhances the thermal emission.

## 2 Thermal Extractor with Natural Material

As an experimental demonstration of the above theory, we discuss here the experiment that uses a carbon-black thermal body as the emitter [8]. It has an index of $n_i$= 2.3 and an emissivity around 0.85 in the near-infrared to mid-infrared region. A circular carbon dot is coated on a polished aluminum sample holder, which provides a low emission background. A hemispherical dome made from ZnSe is used as the thermal extractor. It has an index of $n_e$ = 2.4 and is transparent in the near-infrared to mid-infrared region. The dome's radius is chosen such that the condition R > $n_e$r is satisfied.

The aluminum sample holder is placed on a temperature controlled heater (Fig. 2c,d). The entire heater is placed in a vacuum chamber ($\sim 10^{-6}$Torr) to avoid oxidation of ZnSe and to maintain thermal stability. The thermal radiation is measured through a $CaF_2$ window on the vacuum chamber. The thermal emission is collected by a parabolic mirror and sent through an aperture to a Fourier transform infrared (FTIR) spectrometer. To measure the angular emission, the heater stage can be rotated inside the vacuum chamber. For calibration purposes, a blackbody simulator (Infrared System Development Corporation 564/301 and IR-301 Blackbody controller) is also measured using the same optical set-up. Background emission from the aluminum sample holder has been subtracted in the data shown below.

Figure 5 shows the emission spectra of the structures at various angles. The spectral density from an ideal blackbody of the same size as the carbon black dot is plotted as reference (black lines). As expected, the bare carbon dot (blue lines) emits less than the ideal blackbody, with an emissivity of 0.85 in the normal direction. In the presence of the dome, the emitted power in the normal direction from the same carbon-black dot is enhanced by 4.46-fold, representing a 3.79-fold enhancement over the emission by an ideal blackbody with the same area as the carbon-black dot (Fig. 5a). Similar enhancement is observed for

Brought to you by | University of Wisconsin Madison Libraries
Authenticated
Download Date | 6/3/16 6:36 PM

off-normal directions as well (Fig. 5b–d). The experiment also shows that the enhanced emission is purely from the extraction of carbon's internal thermal energy, not from the ZnSe hemisphere.

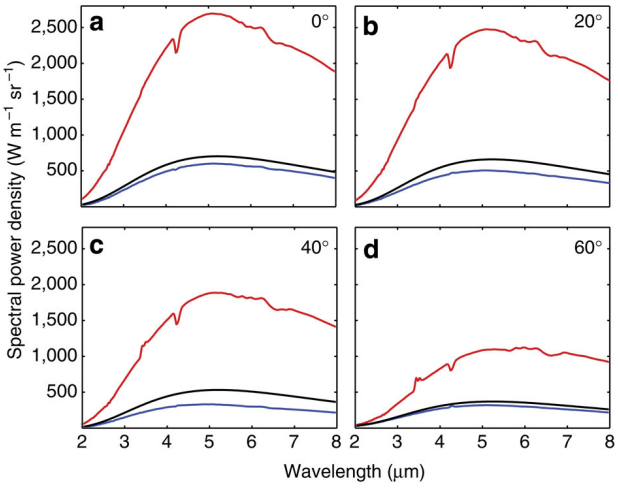


**Figure 5:** Emitted power spectra measured at 553 K for different collection angles. Red and blue lines are for the carbon dot with and without the hemispherical dome, respectively. Black lines are emission power from an ideal blackbody of the same area as the carbon dot at the same temperature. The ripples in the curves are caused by atmosphere absorption. (a), (b), (c), and (d) are measured at 0 degrees, 20 degrees, 40 degrees, and 60 degrees, respectively [8].

Fig. 6 shows the angular emission, as obtained by integrating the spectral density over the wavelength range of 2–8 μm. For all angles, the presence of the dome results in enhanced emission (Fig. 6 red curve), as compared with both the carbon-black dot without the dome (Fig. 6, blue curve) and an ideal thermal body (Fig. 6, black curve) of the same area. The total thermal emission is obtained by integrating over all angles and all wavelengths in the range of 2–8 μm. The total emission is 10.4 mW for the ideal thermal body, 7.6 mW for the bare carbon dot and 31.3 mW for the carbon dot with the dome.

To achieve maximum thermal extraction, we require that all evanescent waves from the emitter can couple into the dome. Thus the emitter and the dome must be in optical contact, that is, the distance between the emitter and the flat surface of the dome must be significantly smaller than the thermal wavelength. If the distance between the emitter and the dome is much larger than the thermal wavelength, thermal extraction does not work. An example of a distance of 30 μm is shown by the green line in Fig. 6. In the normal direction, due to the focusing effect of the hemispherical dome, the emission is higher than that that of bare carbon dot, but it quickly diminishes at

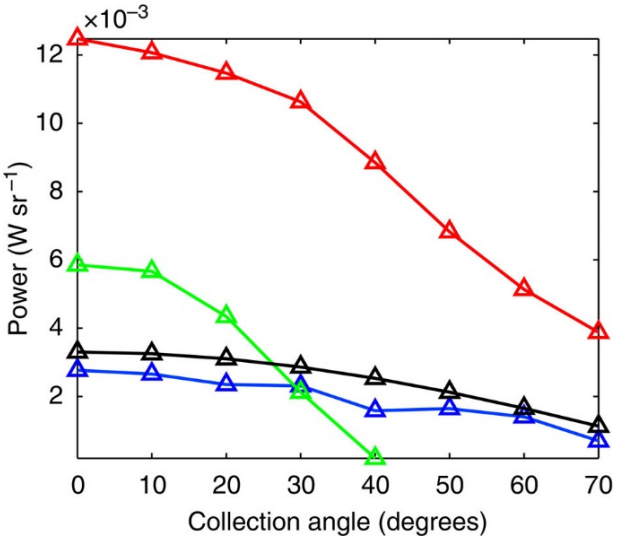


**Figure 6:** Experimentally measured emission power from the carbon dot as a function of angle. Red and blue is for with and without the ZnSe hemispherical dome in optical contact, respectively. Green is for the case where the flat surface of the dome is separated from the carbon dot by 30 μm. Triangles are measured data points. The black line is the emission power from an ideal blackbody with the same area as the carbon dot [8].

large angles with negligible emission beyond 40 degrees. The total emitted power is only 4.1 mW below that from the ideal thermal body with the same area at the same temperature.

## 3 Thermal Extractor with Structured Material

As shown in Eq. (1) the maximum enhancement of the dome-like extraction devices is limited by $n_e^2$ times of the blackbody radiation limit for $n_e<n_i$. This limitation can be overcome by using structured materials to realize much higher effective refractive indices. Here we discuss the experimental work that uses hyperbolic metamaterials (HMs) for thermal extraction, which can significantly enhance near-field energy transfer by extracting evanescent waves with arbitrarily large lateral wave vectors. As a special class of indefinite media, HMs with the principal components of the permittivity tensor $\epsilon$ having opposite signs have a dispersion relation that satisfies a hyperbolic function (red curves in Fig. 7a):

$$\frac{(k_z^2)}{\epsilon_{x,y}} - \frac{K^2}{|\epsilon_z|} = k_0^2 \tag{4}$$

Brought to you by | University of Wisconsin Madison Libraries
Authenticated
Download Date | 6/3/16 6:36 PM

where $\epsilon_z$is the vertical component ($\epsilon_z$<), $\epsilon_{x,y}$ is the lateral component ($\epsilon_{x,y}$>) with the materials assumed to be uniaxial (i.e.,$\epsilon_x$=$\epsilon_y$=$\epsilon_{x,y}$), $k_z$ and K are the vertical and lateral components of the wavevector, respectively.

If a point source is located near an HM, its emitted evanescent waves in vacuum (wavevector $k = \sqrt{k_z^2+K^2} > k_0$) can excite propagating modes in the HM, leading to enhanced photon local density of states (PLDOS). Thus if a lossless HM (i.e., a real permittivity tensor $\epsilon$) is placed between the emitter and the absorber, and is in optical contact with the emitter as a thermal extraction device, evanescent waves from the emitter can be converted into propagating waves in the HM and transfer energy from the emitter to the absorber. In comparison with the extraction device for far-field emission [8], an ideal HM extractor could greatly enhance the rate of radiative heat transfer far beyond what nature materials could offer. As discussed above, HMs are not the only choice here. Any structured material that possesses a large PLDOS can be used as an effective thermal extractor. To realize HMs, metal wire arrays (MWAs) have been chosen from all other possibilities in this demonstration because metamaterials made from MWAs are extremely low-loss and can maintain the hyperbolic dispersion in a broad frequency band within the infrared regime [42]. Particularly, MWAs were demonstrated to have a dispersion relation of $k_z = \sqrt{\epsilon_{x,y}} k_0$, which corresponds to a HM with $\epsilon_z = \infty$, reducing the hyperbolic function to two flat lines (blue dashed lines in Fig. 7a) [42]. As a result, MWAs perform as lossless waveguides that can duplicate the exact field profiles at one end and transfer them to the other end.

To quantitatively evaluate the performance of MWAs as a near-field thermal extractor, the PLDOS is studied for structures with different thickness and each compared with corresponding cases without MWAs (Fig. 7c). It has been shown that the calculated PLDOS at a distance of 100 nm above the HM slab can be enhanced by one order of magnitude, compared with the PLDOS at the same location without the HM slab and that the wave-guiding properties or the HM characteristics of MWAs are almost independent of the wire length, as long as the period of the wires is much smaller than the lateral wavelength of incident photons. The HM modes in MWAs are extremely low-loss because electromagnetic energy is highly concentrated on metal wire surfaces with little penetration. The decay length of MWAs is estimated to be much longer than the wavelength. Fig. 7d shows the electric field profile excited by a dipole located at a 100 nm distance above the 500 nm thick slab. The uniform field distribution along the wires further confirms the waveguiding effect of MWAs.

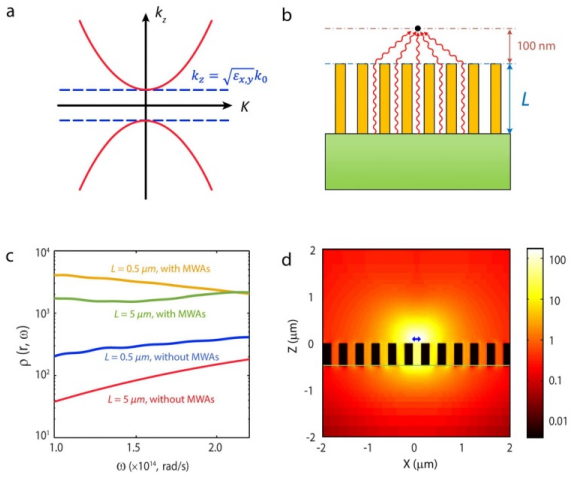


**Figure 7:** Hyperbolic metamaterials (HMs) mediated near-field thermal extraction. (a) Dispersion relation of typical HMs (red curves) and metal wire arrays (MWAs) (blue dashed lines). (b) Schematic of the MWA-based near-field thermal extractor. (c) Calculated photon local density of states (PLDOS) at 100 nm above MWAs for different lengths $L$ =500 nm and $L$ =5 μm with/without the MWAs. (d) Electric field intensity excited by a dipole located at 100 nm above the 500 nm thick slab of MWAs [9].

The experiment demonstration is done by measuring the radiative heat transfer between a microsphere and a substrate at nanoscale gaps (Fig. 8a,b). To probe the heat transfer, a $SiO_2$ microsphere is attached to the tip of a bimaterial ($SiN_X$/gold) atomic force microscope cantilever, which is very sensitive to temperature and therefore can resolve heat power as small as 0.1 nW [55, 56]. A laser beam is used to measure the deflection of the cantilever and heat the microsphere to $\sim 50\,^\circ$, whereas the sample substrate is maintained at ambient temperature. When the sphere approaches the substrate, the heat flow radiated from the microsphere to the substrate greatly increases due to near-field heat transfer [31, 32] and causes the bending of the cantilever by reducing the temperature of the sphere. As shown in Fig. 8c inset, the deflection signal of the cantilever, which also represents the near-field heat transfer signal, increases as the gap decreases with time. The sharp change in the slope of cantilever deflection signals indicates the mechanical contact between the sphere and the substrate (Fig. 8c), thereby providing a reference to precisely determine the substrate-sphere separation.

To fabricate the MWA-based HMs, we employ anodic aluminum oxide (AAO) nanoporous templates to grow vertically aligned metal nanowires via electrochemical deposition [57–59]. Fig. 9a,b show nickel nanowire arrays embedded in an AAO template. To prove that MWAs only participate in heat transfer as a passive waveguide, the near-

Brought to you by | University of Wisconsin Madison Libraries
Authenticated
Download Date | 6/3/16 6:36 PM

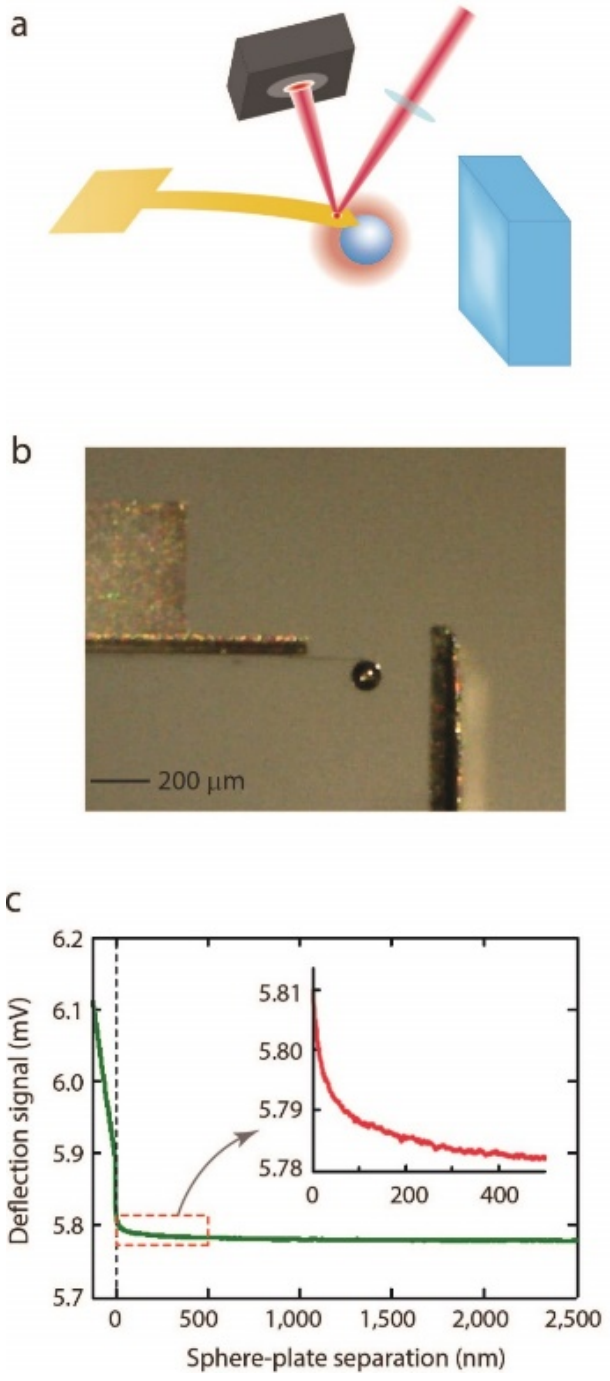


**Figure 8:** Experimental set-up for near-field thermal measurements. (a) Schematic of the experiment set-up that shows the relative position between the optical deflection system and the sample. (b) Optical image of the set-up. (c) Typical cantilever deflection signals when the sphere approaches the substrate. The contact point between the sphere and the plate is marked by the vertical dashed black line. Inset: Deflection signals close to the contact point [9].

field radiative heat flux between the $SiO_2$ microsphere and bare nickel nanowire arrays in vacuum supported on a ~30 μm thick nickel film was measured. The temperature difference between the $SiO_2$ sphere and the nickel nanowires was calibrated to be 29 K. The $SiO_2$ microsphere serves as a super-Planckian near-field absorber/emitter (with a very large PLDOS close to its surface) [32] and the nickel film beneath the nanowires performs as a mirror – an extremely inefficient thermal emitter/absorber.

It has been demonstrated that the near-field heat transfer between an $SiO_2$ sphere and a metal surface is almost zero [32]. If substantial heat transfer occurs between the $SiO_2$ sphere and the nickel nanowires, it must be attributed to the contribution from the nickel nanowires rather than the 30 μm thick nickel film. However, there is no obvious heat transfer observed (Fig. 9c). This is because the nanowires are low-loss for thermal radiation, and therefore the propagating waves along the 10 μm long nanowires have negligible dissipation. On the other hand, when the non-decaying propagating waves reach the highly reflective nickel film at the end of the nanowires, they will be almost totally reflected. As a result that nickel nanowire array can work as a passive lossless waveguide for thermal radiation.

To measure near-field thermal extraction MWAs are connected with a lossy thermal emitter/absorber instead of a metal mirror in the above case. To demonstrate near-field thermal extraction effect, we measure the near-field heat transfer with/without the protruded nickel nanowires as a thermal extractor. In Fig. 10c, where near-field thermal conductance is plotted as a function of the gap d between the $SiO_2$ sphere and the absorbing substrate (Fig. 10c, upper right inset), the HM thermal extractor can dramatically enhance near-field heat transfer. At the smallest separation between the sphere and the nanowires, the measured thermal conductance with the protruded nanowires is around one order of magnitude larger than the case without the protruded nanowires. This result demonstrates the excellent near-field thermal extraction performance of MWAs. It is worth noting that in order to demonstrate the near-field thermal extraction effect of MWAs, the near-field emitters and absorbers can be arbitrarily chosen.

Near-field thermal extraction of MWAs is independent of the material properties of emitters/absorbers. For any thermal emitters/absorbers, such as a lossy AAO template or a $SiO_2$ sphere in this work, they all support thermally excited evanescent waves. When the emitter and the absorber are separated by a large gap compared with the wavelength of thermal radiation, the evanescent modes exponentially decay from the surface and do not contribute to heat transfer. However, if an HM (e.g., MWAs) is

Brought to you by | University of Wisconsin Madison Libraries
Authenticated
Download Date | 6/3/16 6:36 PM

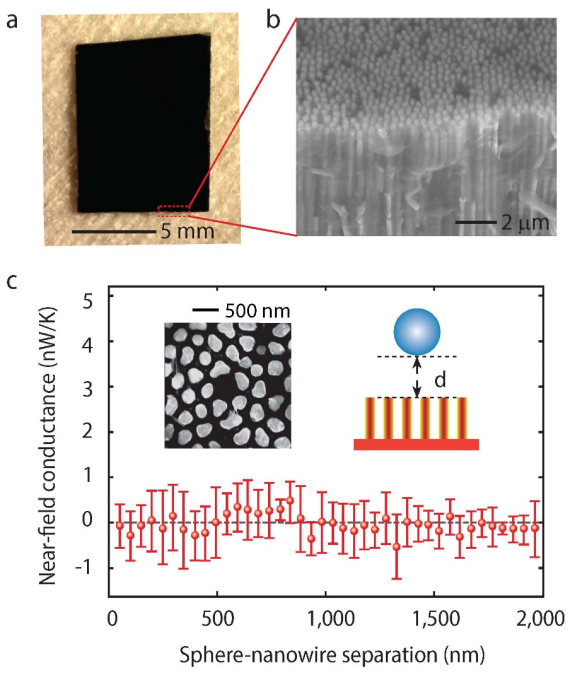


**Figure 9:** Fabrication of a hyperbolic metamaterial (HM) composed of metal wire arrays (MWAs) and its application as low-loss waveguides. (a) Optical image of the polished nickel nanowire-anodic aluminum oxide (AAO) composite. (b) SEM image of the side view of the polished sample shown in (a). (c) Near-field heat transfer between an $SiO_2$ sphere and free-standing nanowire arrays as a function of nanowire-sphere separation. The dashed line indicating zero near-field conductance is drawn for eye guidance. The upper left inset is the SEM image of the top view of free-standing nanowires, where the nanowires are well separated from each other after supercritical drying [9].

optically contacted with the emitter and placed between the emitter and the absorber, the evanescent modes from the emitter can be converted into the propagating modes in the HM, and then transfer energy to the absorber. Hence radiative heat transfer can be greatly enhanced by the extracted evanescent modes.

Lastly, we note that thermal extractors do not require completely lossless materials. In fact, lossy materials can also be used as thermal extractors as long as the propagation length of thermal photons is longer than the optical path length that is needed in order to reach the outside vacuum. For low-temperature applications such as at T <500 K, the wavelength of thermal photons is in the mid-infrared region where metals have much lower optical loss than in the visible wavelength range. Therefore, many metamaterials that are based on metallic structures could be used as thermal extractors to realize extraordinarily high density of states and thermal extraction enhancement.

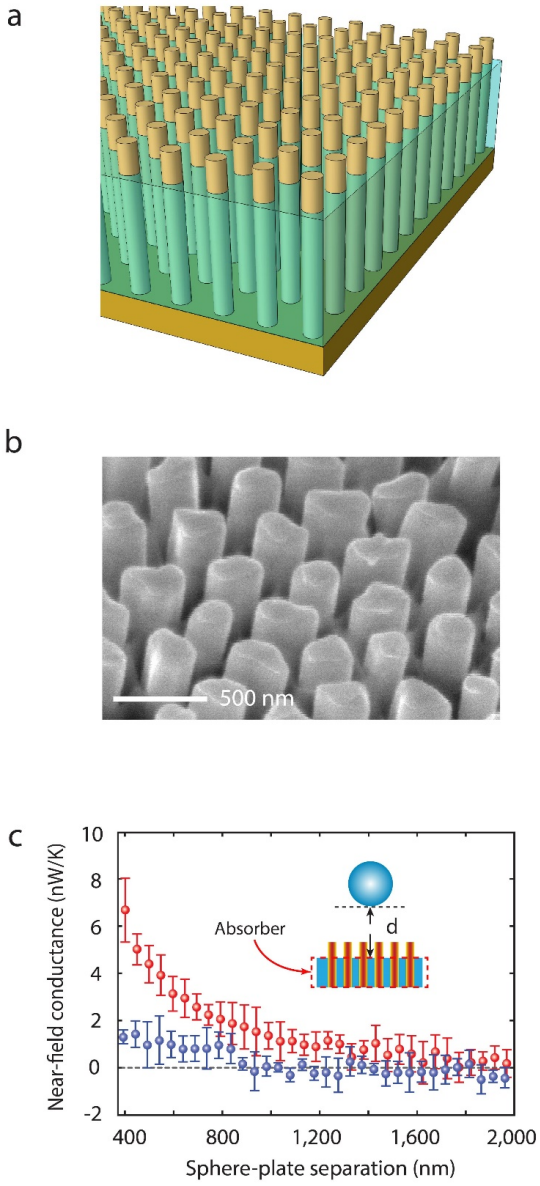


**Figure 10:** Experimental demonstration of near-field thermal extraction. (a) Schematic and (b) SEM image of partially released nickel nanowire arrays. The protruded nanowires are measured to be ~400 nm from the anodic aluminum oxide (AAO) template. (c) Near-field heat transfer as a function of the gap between the sphere and the AAO template with (red dots) and without (blue dots) the protruded nanowires. The dashed line indicating zero near-field conductance is drawn for eye guidance. The separation between the sphere and the substrate (AAO template) ends at ~400 nm because of the protruded nanowires [9].

## 4 Conclusion

We have reviewed the concept of thermal extraction with the example of a high-index hemispherical dome and metallic nanowire metamaterials. In general, thermal ex-

Brought to you by | University of Wisconsin Madison Libraries
Authenticated
Download Date | 6/3/16 6:36 PM

traction can be accomplished with other geometries as well. Here we comment on the general requirement of the thermal extraction device: Firstly, the thermal extraction needs to be in optical contact with the emitter, that is, the distance between the emitter and the extraction device needs to be smaller compared with the evanescent length scale determined by the thermal wavelength. This is to ensure that all internal states in the emitter can couple to modes in the extraction device. We note, however, the thermal extraction device need not be in physical contact with the emitter. This could be useful in practice when it is advantageous to prevent thermal conduction between the extraction device and the emitter. Secondly, from a thermodynamics point of view, the thermal extraction device needs to provide enough radiation channels over the area of the emitter to ensure that all internal modes of the emitter can outcouple. A simple way to accomplish this is to choose the extraction device such that its density of states is larger than that of the emitter. The size of the extraction device also needs to be sufficiently large, such that the vacuum region immediately outside the extraction device has sufficient number of radiation channels to accommodate all the thermal emission. Both of these considerations are incorporated in our choice of parameters for the hemispherical dome. On the other hand, based upon these considerations, one can envision a wide variety of nanophotonic structures that may satisfy these thermodynamic considerations. Finally, in the extraction device those optical modes that receive radiation from the emitter need to be accessible to far-field vacuum. This places a constraint on the geometry of the extraction device. For example, a transparent high-index slab with a flat surface does not provide thermal extraction. Even though more radiations can enter the slab, those outside the escape cone defined by $\sin 1(1/n_e)$ cannot escape to far-field vacuum due to total internal reflection. As a result, the total far-field emission remains the same as $S\sigma T^4$. This particular requirement of making internal optical states accessible to far-field shares the same spirit of the requirement of light trapping in solar cells. Many light trapping structures, for example, roughened slab, irregular polygon and nanostructured interface can be directly used for thermal extraction.

**Acknowledgement:** The work is supported by National Science Foundation (Nos. ECCS-1405201 and CBET-1253692.

## References

[1] Tong, J., et al. Infrared-transparent visible-opaque Fabrics for wearable personal thermal management. *ACS Photonics,* **2** (2015): 769

[2] Guo, Y., et al. Broadband super-Planckian thermal emission from hyperbolic metamaterials. *Applied Physics Letters,* **101** (2012): 131106.

[3] Volokitin, A. I., et al. Near-field radiative heat transfer and noncontact friction. *Reviews of Modern Physics,* **79** (2007): 1291.

[4] Hu, L., et al. Near-field thermal radiation between two closely spaced glass plates exceeding Planck's blackbody radiation law. *Applied Physics Letters*, **92**(2008): 133106.

[5] Narayanaswamy, A.,et al. Near-field radiative heat transfer between a sphere and a substrate.*Physical Review B,* **78** (2008): 115303.

[6] Joulain, K., el al. Surface electromagnetic waves thermally excited: Radiative heat transfer, coherence properties and Casimir forces revisited in the near field. *Surface Science Reports*, **57** (2005): 59-112.

[7] Zhang, Zhuomin M. *Nano/microscale heat transfer.* New York: McGraw-Hill, 2007.

[8] Yu, Z., et al. Enhancing far-field thermal emission with thermal extraction. *Nature Communications,* **4** (2013): 1730

[9] Shi, J., et al. Near-field energy extraction with hyperbolic metamaterials. *Nano Letters,* **15** (2015): 1217

[10] Greffet, J. -J. Applied physics: controlled incandescence. *Nature* **478**(2011): 191–192.

[11] Cornelius, C. M. & Dowling, J. P. Modification of Planck blackbody radiation by photonic band-gap structures. *Physical Review A,* **59** (1999): 4736–4746.

[12] Maruyama, S., et al. Thermal radiation from two-dimensionally confined modes in microcavities. *Applied Physics Letters*. **79** (2001): 1393–1395.

[13] Greffet, J. -J. et al. Coherent emission of light by thermal sources. *Nature* **416** (2002):61–64.

[14] Pralle, M. U. et al. Photonic crystal enhanced narrow-band infrared emitters. *Applied Physics Letters*. **81** (2002): 4685–4687.

[15] Fleming, J. G., et al. All-metallic three-dimensional photonic crystals with a large infrared bandgap. *Nature* **417** (2002):52–55.

[16] Lin, S. Y., et al. Three-dimensional photonic-crystal emission through thermal excitation. *Optics Letters* **28** (2003): 1909–1911.

[17] Luo, C., et al. Thermal radiation from photonic crystals: a direct calculation. *Physical Review Letters* **93** (2004): 213905.

[18] Lee, B. J., et al. Coherent thermal emission from one-dimensional photonic crystals. *Applied Physics Letters*. **87** (2005): 071904–071903.

[19] Celanovic, I., et al. Resonant-cavity enhanced thermal emission. *Physical Review B,* **72** (2005): 075127.

[20] Laroche, M., et al. Highly directional radiation generated by a tungsten thermal source. *Optics Letters*. 30 (2005): 2623–2625.

[21] Dahan, N., et al. Enhanced coherency of thermal emission: beyond the limitation imposed by delocalized surface waves. *Physical Review B,* **76** (2007): 045427.

[22] Wang, C. -M., et al. Reflection and emission properties of an infrared emitter. *Optics Express* **15** (2007): 14673–14678.

[23] Puscasu, I. &Schaich, W. L. Narrow-band, tunable infrared emission from arrays of microstrip patches. *Applied Physics Letters*,

Brought to you by | University of Wisconsin Madison Libraries
Authenticated
Download Date | 6/3/16 6:36 PM

**92** (2008): 233102.
[24] Rephaeli, E. & Fan, S. Absorber and emitter for solar thermophotovoltaic systems to achieve efficiency exceeding the Shockley-Queisser limit. *Optics Express,***17** (2009): 15145–15159.
[25] Liu, X., et al. Taming the Blackbody with infrared metamaterials as selective thermal emitters. *Physical Review Letters,***107** (2011): 045901.
[26] Yeng, Y. X., et al. Enabling high-temperature nanophotonics for energy applications. *Proceedings of the National Academy of Science, USA*, (2012) 1120149109.
[27] De Zoysa, M. et al. Conversion of broadband to narrowband thermal emission through energy recycling. *Nature Photonics,* **6** (2012): 535–539.
[28] Schuller, J. A., et al. Optical antenna thermal emitters. *Nature Photonics*. **3** (2009): 658–661.
[29] Polder, D. & Van Hove, M. Theory of radiative heat transfer between closely spaced bodies. *Physical Review B,***4** (1971): 3303–3314.
[30] Pendry, J. Radiative exchange of heat between nanostructures.*Journal of Physics: Condensed Matter,***11** (1999): 6621–6633.
[31] Rousseau, E. et al. Radiative heat transfer at the nanoscale. *Nature Photonics*. **3** (2009)514–517.
[32] Shen, S., et al. Surface phonon polaritons mediated energy transfer between nanoscale gaps. *Nano Letters,***9** (2009): 2909–2913.
[33] Winston, R., et al. *Nonimaging Optics*, 18 (AcademicPress, 2004).
[34] Carr, W. N. & Pittman, G. E. One-watt GaAs p-n junction infrared source. *Applied Physics Letters*. **3** (1963): 173–175.
[35] Moreno, I., et al. Light-emitting diode spherical packages: an equation for the light transmission efficiency. *Applied Optics,***49** (2010): 12–20.
[36] Terris, B. D., et al. Near-field optical data storage using a solid immersion lens. *Applied Physics Letters*. **65** (1994): 388–390.
[37] Siegel, R. & Howell, J. R. *Thermal Radiation Heat Transfer*, 37 (Hemisphere Publishing Corporation, 1992) & (Taylor & Francis: London, 2001).
[38] Yu, Z., Raman, A. & Fan, S. Fundamental limit of nanophotonic light trapping for solar cells. *Proceedings of the National Academy of Science, USA,***107** (2010): 17491–17496.
[39] Yablonovitch, E. Statistical ray optics. *Journal of Optical Society of America A,***72** (1982): 899–907.
[40] Campbell, P. & Green, M. A. Light trapping properties of pyramidally textured surfaces. *Journal of Applied Physics*. **62** (1987): 243–249.
[41] Catalanotti, S. et al. The radiative cooling of selective surfaces. *Solar Energy,***17** (1975):83–89.
[42] Liu, B., et al. Broadband near-field radiative thermal emitter/absorber based on hyperbolic metamaterials: Direct numerical simulation by the Wiener chaos expansion method. *Physical Review B,***87** (2013): 115403.
[43] Otey, C. R. et al. Phys. Rev. Lett. 2010, 104, 154301.
[44] Byrnes, S. J, et al. Harvesting renewable energy from Earth's mid-infrared emissions. *Proceedings of the National Academy of Science, USA*. **111** (2014): 3927–3932.
[45] Padture, N. P, et al.Thermal Barrier Coatings for Gas-Turbine Engine Applications. *Science*. **296** (2002): 280–284.
[46] Ben-Abdallah, P., et al. Near-Field Thermal Transistor. *Physical Review Letters*.**112** (2014): 044301.
[47] Biehs, S.-A, et al. Mesoscopic Description of Radiative Heat Transfer at the Nanoscale. *Physical Review Letters*. **105** (2015): 234301.
[48] Messina, R., et al. Graphene-based photovoltaic cells for near-field thermal energy conversion. *Scientific Reports*. **3** (2013): 1383.
[49] Guha, B., et al. Near-Field Radiative Cooling of Nanostructures. *Nano Letters*. **12** (2012): 4546–4550.
[50] De Wilde, Y., et al. Thermal radiation scanning tunnelling microscopy.*Nature.***444** (2006): 740–743.
[51] Challener, W. A.,et al. Heat-assisted magnetic recording by a near-field transducer with efficient optical energy transfer. *Nature Photonics.***3** (2009): 220–224.
[52] Poddubny, A., et al. Hyperbolic metamaterials. *Nature Photonics.***7** (2013): 948–957.
[53] Shvets, G., et al. Guiding, Focusing, and Sensing on the Subwavelength Scale Using Metallic Wire Arrays. *Physical Review Letters*.**99** (2007): 053903.
[54] Joulain, K., et al. Definition and measurement of the local density of electromagnetic states close to an interface. *Physical Review B,***68** (2003): 245405.
[55] Barnes, J. R., et al. A femtojoule calorimeter using micromechanical sensors. *Review of Scientific Instruments*.**65** (1994): 3793–3798.
[56] Narayanaswamy, A.; Gu, N. Heat Transfer From Freely Suspended Bimaterial Microcantilevers. *Journal of Heat Transfer*.**133** (2011): 042401.
[57] Yao, J., et al. Design, fabrication and characterization of indefinite metamaterials of nanowires. *Mathematical, Physical and Engineering Science*. **369** (2011): 3434–3446.
[58] Nielsch, K., et al. Uniform Nickel Deposition into Ordered Alumina Pores by Pulsed Electrodeposition. *Advanced Materials*. **12** (2000): 582–586.
[59] Chen, R., et al. Nanowires for Enhanced Boiling Heat Transfer. *Nano Letters*. **9** (2009): 548–553.
[60] Du, T., et al. Chemical mechanical polishing of nickel for applications in MEMS devices. *Microelectronic Engineering.***75** (2004): 234–241.
[61] Shi, J., et al. Tuning near field radiation by doped silicon. *Applied Physics Letters*. **102** (2013): 183114.
[62] Carr, W. N. & Pittman, G. E. One-watt GaAs p-n junction infrared source. *Applied Physics Letters*.**3** (1963): 173–175.

Brought to you by | University of Wisconsin Madison Libraries
Authenticated
Download Date | 6/3/16 6:36 PM